A NUMERICAL CONCEPT STUDY ON INTERNAL BLADE COOLING IN AXIAL COMPRESSORS

T. Willeke - M. Hellberg - J. R. Seume

Institute of Turbomachinery and Fluid Dynamics
Leibniz Universität Hannover
Appelstraße 9, 30167 Hannover, Germany
willeke@tfd.uni-hannover.de

ABSTRACT

The stator blades of a three-stage axial compressor were equipped with internal cooling channels to investigate the effects of internal blade cooling on axial compressor performance and gas-turbine efficiency. For water-cooled stator blades under realistic boundary conditions, the results from numerical simulations predict an isentropic total-to-total stage efficiency increase by 1.26 percentage points with no effect on the stage pressure ratio. In terms of overall efficiency, a multi-stage axial compressor profits from internal stator-blade cooling by a 1.45% increase. Increasing the heat exchanging surface through a higher stator solidity, this cooling benefit surpasses higher blade losses, and can be further maximized for high solidity stators. Gas-turbine efficiency, with or without recuperation is predicted to be directly proportional to the improvements in compressor efficiency.

KEYWORDS

STATOR, STAGE, EFFICIENCY, COOLANT, HEAT

NOMENCLATURE

A	area	c, c_p	heat capacity	D	diameter
l	length	$\dot{m}$	mass flow	P	power
p	pressure	$\dot{Q}$	cooling rate	$\dot{q}$	heat flux
T	temperature	u	flow velocity	$\dot{V}$	volume flow
α	heat transfer coefficient	γ	heat capacity ratio	η	isentropic tot-tot efficiency
λ	thermal conductivity	μ	viscosity	π	total-total pressure ratio
ρ	density	ξ	loss factor	ω	pressure-loss coefficient

$Re = \frac{\rho u D}{\mu}$ Reynolds number $Pr = \frac{\mu c_p}{\lambda}$ Prandtl number $Nu = \frac{\alpha D}{\lambda}$ Nusselt number

INTRODUCTION

Gas turbines for industrial applications and aircraft engines generate work output in the form of rotating shaft power or thrust for propulsion through the real Joule cycle. This thermodynamic cycle combines a polytropic compression of the working fluid, with an ideally isobaric heating followed by a polytropic expansion. The specific work output of the real gas-turbine cycle depends not only on the cycle efficiency and the total pressure ratio, but also on the turbine inlet total temperature. Common approaches to maximize the specific work output are higher pressure ratios and higher turbine inlet temperatures.

Technological limits to this trend are set by the mechanical strength and thermal resistance of component materials, blade materials in particular. To protect turbomachinery components

against thermally induced failure, the endangered machine parts are cooled by 3 to 5% of compressed air which is extracted from the primary flow (Han et al., 2013). Thermodynamically, component cooling during compression or expansion leads to smaller temperature differences across the cooled component, and a lower specific work by this component. Nevertheless, internal and external cooling of rotating and stationary blades in the first stage of high pressure turbines is a standard feature in modern gas turbines, because of the work increase which is achieved by higher inlet temperatures up to 1700°C (Han et al., 2013) and which surpasses the amount of work which is sacrificed for cooling.

Increasing the compressor efficiency is another option for further cycle improvements which is widely pursued in industry and research. Projects like *Vision 2020* and *Flightpath 2050* pursue the ambitious objectives of CO_2 and NO_x emissions of aircraft engines by 75% and 90%, respectively. In the *NEWAC* project (Sieber, 2015), researchers try to achieve higher thermal efficiency without increasing temperatures through improvements in component efficiency. Innovative technological concepts, such as active core systems and flow control technologies are accompanied by core-integrated intercoolers and exhaust gas heat exchangers. Referring to Sieber (2015), most *NEWAC* activities are focused on the compressor and are limited to aerodynamic topics, secondary tip-leakage flow improvements in particular.

Moving away from the established aerodynamic focus in compressor-efficiency research, Shah and Tan (2007) compared axial compressor performance with heat extraction via blade passage surfaces to its adiabatic counterpart, using results from two-dimensional CFD simulations with *FLUENT* and mean-line analyses. The axial compressors under consideration were the *NASA Rotor 35* for three-dimensional analysis, and a single-stage fan and an eight-stage compressor with a pressure ratio of 5 for a Mach-4 vehicle at 25 km flight alltitude for mean-line analysis. For the simulation of the *NASA Rotor 35*, Shah and Tan (2007) used an inlet stagnation temperature of 300 K (27°C), and a wall-temperature boundary condition of 100 K (-173°C) on the blade surface and at the rotor casing wall. They found that compressor cooling would raise the overall pressure ratio at a given corrected flow, the maximum mass flow capability, and the efficiency defined as the ratio of isentropic work for a given pressure ratio to actual shaft work. It would also provide rear stage choking relief at low corrected speed. Results from their single-stage fan studies show that the increase in overall pressure ratio can be attributed to both the increase in stagnation pressure from cooling and the increase in flow turning. Shah and Tan (2007) conclude that a given amount of cooling in the front is better than in the rear. Nevertheless, they point out that higher blade solidity and the ratio of wall temperature to the main-flow stagnation temperature are higher in the rear stages. They indicate that for a given compressor, an optimal stagewise cooling distribution should exist based upon cycle and compressor geometry, which leaves an open design problem for future work.

On this basis, this paper summarizes the results of numerical aero-thermal studies for a simple concept for internal blade cooling in axial compressor blades. This concept study emerged from the authors' very basic interest in some figure of merit for the feasibility of cooling in axial compressor blades and attributes some valuable information to the open questions posed by Shah and Tan (2007) on an engineering level. For this purpose, an internally cooled compressor blade is designed and the internal cooling flow in a single blade is analyzed in terms of surface heat flux and coolant pressure loss. An analytical model expands these results for further cooling configurations with adjacent blades and stages. The cooling effect on pressure ratio and efficiency is investigated for a single stage and a three-stage axial compressor. Finally, the cycle efficiency gain by cooling with and without recuperation is predicted.

Table 1: **Design specifications of baseline compressor**

Flow coefficient	ϕ	-	0.49
Load coefficient	ψ	-	0.74
Isentropic efficiency	η_s	-	0.88
Rotational speed	N	rpm	15,000
Tip radius	r_{tip}	mm	170

Table 2: **Stator-blade parameters**

			S1	S2	S3
Number of blades	z	-	24	26	28
Profile shape	-	-	*NACA 65*	*NACA 65*	*NACA 65*
Surface area	A_{blade}	mm^2	6,775	5,154	3,857
Blade height	h_{blade}	mm	75	58	48
Chord length	c	mm	42	40	36
Wall temperature	T_{wall}	K	303	319	337
Wall pressure	p_{wall}	Pa	109	127	149

ANALYSIS OF A SINGLE INTERNALLY COOLED STATOR BLADE

Design of an Internally Cooled Stator Blade

The first design decision is to limit the blade cooling to stator blades only. Because of the high mechanical stresses experienced by rotor blades, these blades do not have much of a material-strength reserve to carry additional thermal stresses from cooling-induced temperature gradients.

The second decision is to use an existing blade design of a multi-stage axial compressor, which is comparable to conventional high-pressure compressors. Moreover, a special blade design adapted to the aerodynamic and mechanical characteristics of a cooled compressor requires suitable and reliable design rules for the prediction of blade-cooling effects in axial compressors. The latter is unavailable initially. The three-stage axial compressor design used for the baseline configuration was designed by the first author. As of this writing, experimental validation of this compressor has not been completed. Design parameters which are relevant for the present work are given in Table 1.

A stator blade from the second stage is chosen as the reference blade for the design of an internally cooled blade. Because the second stage is the middle stage of the three-stage compressor, it has a representative character in terms of geometry dimensions and aerodynamic properties. Thus, it represents a suitable compromise between the maximum blade-surface area of the first-stage blades, and the maximum flow temperature in the third-stage.

The decision for an internal cooling mechanism is made mainly because of engineering considerations and the simplicity of this preliminary concept study. Since similar compressor blades of another axial compressor have been equipped with internal cavities for pressure-tap instrumentation and active flow control (AFC), experimentally proven rules for their mechanical

Table 3: **Blade material and coolant fluids**

Material	Density ρ in kg/m^3	Heat capacity c, c_p in $J/(kg \cdot K)$	Heat conductivity λ in $W/(m \cdot K)$	Viscosity μ in $10^{-3} kg/(m \cdot s)$
X20Cr13	7,712	465	22.5	-
Water	997	4,182	0.607	0.89
Jet-A1	790	2,338	0.116	1.41
Air	1.18	1,004	0.026	0.018

design exist. These design rules are simply adopted for the cooling purpose. Nevertheless, any external cooling mechanism would also require a coolant supply through the blade interior. Thus, basic internal cooling is the technical predecessor of any concept with external cooling. Aerodynamically, a blade-internal coolant flow does not interact with the compressor main flow. This last aspect might hold further potential or disadvantages for external blade cooling over internal cooling which are beyond the scope of this concept study.

From the numerous concepts for internal cooling, of which many are proven designs for turbine blade cooling, a single cooling channel is chosen for simplicity. This cooling channel has two openings, which are both connected to the casing endwall. This provides an easy access for external coolant supply. Both openings can be chosen for the channel inlet. The cooling channel has a circular cross section with a constant diameter of 1 mm. Internal to the blade, the channel-cross section is located symmetrically around the profile-mean line. The channel starts at the endwall runs radially towards the hub, shifts its direction by 90°, runs back towards the casing, and takes several further U-turns to span the blade in the axial direction. The axial distance over which the meandering channel spreads is limited by the mechanical strength of the remaining blade material between channel and blade surface. Near the leading and the trailing edge, the *NACA-65* profile thickness of the baseline compressor sets these limits for axial spreading. For pressure-tap instrumentation and AFC applications, a material thickness of 0.5 mm defines the lower limit for stainless steel. This restriction in combination with the *NACA-65* profile shape leads to a clustering of the channel loops around the position of maximum blade thickness (Figure 1).

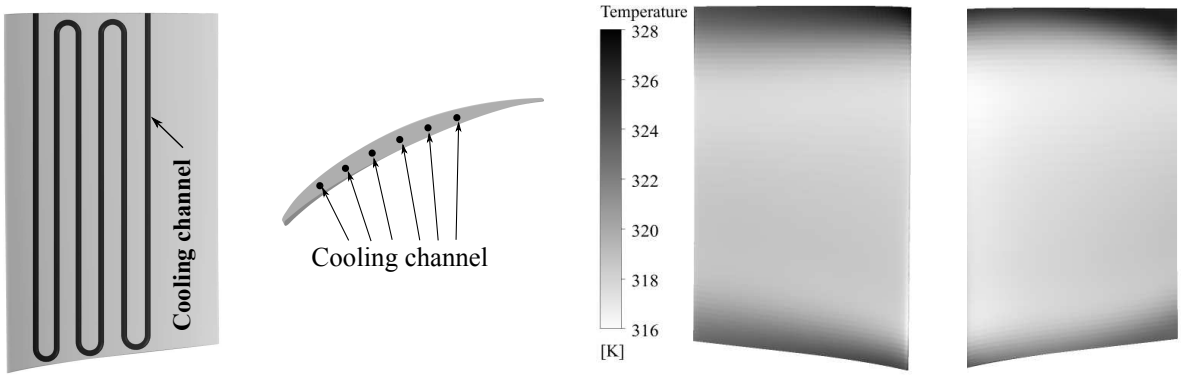

(a) Meridional view (b) Midspan section (c) Pessure side (d) Suction side

Figure 1: **Stator blade with internal cooling channel and wall temperature**

Simulation of the Internal Cooling Flow in a Stator Blade

Numerical Setup

For three-dimensional CFD simulation of the isolated cooled compressor blade, *Ansys CFX* is used to model a fully turbulent flow with the *Shear-Stress-Transport* turbulence model. Conjugate heat transfer is enforced by the blade surface temperature distribution of the adiabatic axial compressor in the aerodynamic design point (Figure 1).

The grid of the stator blade with the internal cooling channel is created with the meshing software *ICEM CFD* resulting in a mesh size of $2.2 \cdot 10^6$ tetrahedrons. Due to high gradients in velocity and temperature, the spatial discretization is refined at the interface between the solid blade body and the fluid body. For this purpose, 12 prism-cell layers with a height ratio

of 1.2 are added on both sides of the interface. The first cell-layer height is chosen to give a dimensional wall distance $y+$ below 2 in regions with attached flow.

Air, kerosene (Jet-A1), and water are considered for coolant fluids. The first two are considered because of their availability in aircraft engines, and the last because of its high heat capacity and heat conductivity (Table 3). All material parameters are held constant for a reference temperature of 25°C. For the internal cooling flow, total pressure, total temperature and a turbulence intensity of 5% are specified at the inlet, whereas the coolant mass flow is defined at the channel outlet.

Results

For various coolants, Figure 2 shows the cooling rate as a function of the pumping power, which is required to drive the coolant through the cooling channel. The coolant flow direction is counter-current to the compressor main-flow direction which means the the channel opening at the trailing edge is chosen for the inlet. Figure 2 reveals that air, kerosene, and water provide significantly different cooling rates for the same pumping power. For a coolant pumping power of 0.5 W, water gives the highest cooling rate of up to 350 W, whereas kerosene and air only attain 35% and 5% of this cooling capability respectively.

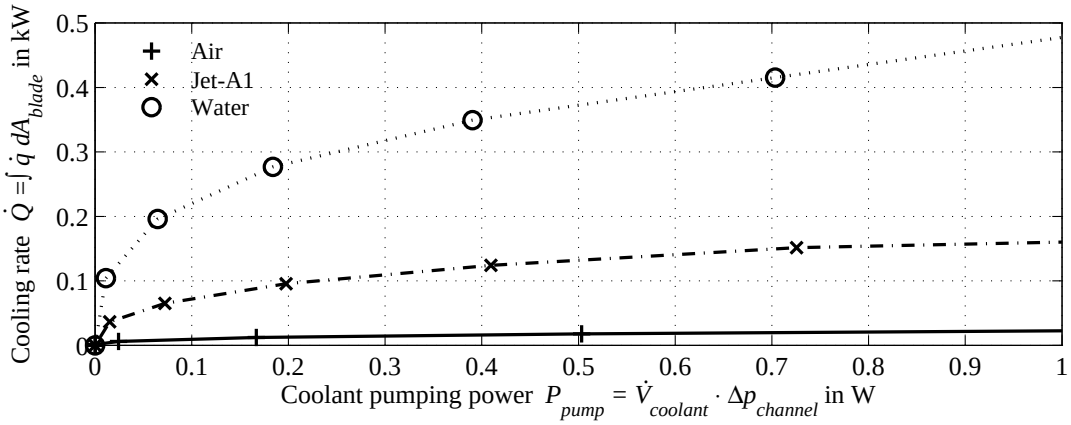

Figure 2: **Coolant pumping power and cooling rate for different coolants**

Figure 3 shows the heat flux distribution on the blade suction side for all coolants at an identical pumping-power level. The coolant flow enters the blade body near the trailing edge and follows the cooling channel in the opposite direction to the external flow around the stator blade. Because of this flow direction and the subsequent increase in coolant temperature, the highest temperature difference and heat flux is present near the trailing edge. Depending on the coolant heat capacity, the cooling effect rapidly diminishes with increasing coolant temperature towards the leading edge. Comparing Figure 2 with Figure 3, the superior cooling capacity of water becomes obvious. In the channel U-bends where the coolant flow cross-flow pattern locally turns directly opposite to the compressor main flow direction, the heat flux increases because of the optimum heat transfer in a counterflow configuration. Comparing Figure 3 with Figures 1(c) and 1(d), the heat exchange between the suction and the pressure side through the thin trailing edge region is visible. This heat transfer is independent of blade cooling but neglected in every adiabatic CFD simulation. The grid-like pattern in the heat-flux distribution is a consequence of a non-matching mapping of the blade surface temperature distribution, from a structured CFD mesh on the unstructured blade-solid grid.

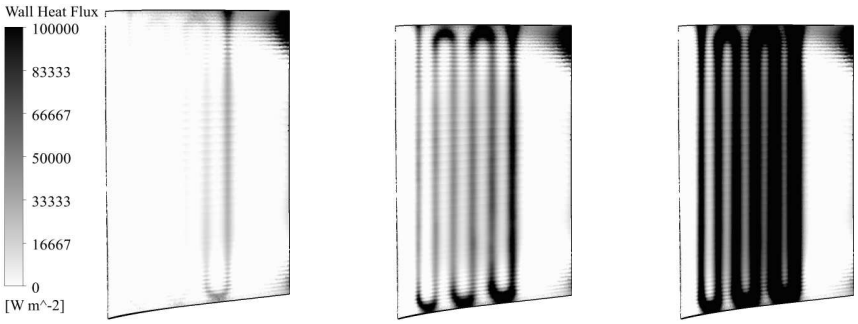

(a) Air (b) Jet-A1 (c) Water

Figure 3: **Wall heat flux for a pumping power of approx. 0.45 W and different coolants**

1D PREDICTION MODEL FOR THE INTERNAL COOLING FLOW

Model Equations

A one-dimensional model is developed for the time-efficient heat transfer prediction of internally cooled stator blades. Because of the thin blades and the superior heat conduction in the blade solid compared to the coolant heat conductivity (Table 3), conductive heat transfer inside the blade body is neglected. In this case and dependent on the coolant-flow Reynolds number Re, the Nusselt number Nu in the cooling channel is estimated by Equation 1 for laminar flow, and Equation 2 for turbulent flow ($Re >$ 2,300) (Gnielinski, 2013).

$$Nu_{m,lam} = \left\{ 3.66^3 + 0.7^3 + \left[1.615 \left(RePr\frac{D}{l} \right)^{\frac{1}{3}} - 0.7 \right]^3 \right\}^{\frac{1}{3}} \tag{1}$$

$$Nu_{m,turb} = \frac{\left(\frac{\xi}{8}\right) RePr}{1 + 12.7\sqrt{\left(\frac{\xi}{8}\right)}(Pr^{2/3} - 1)} \left[1 + \left(\frac{D}{l} \right)^{\frac{2}{3}} \right] \text{ with } \xi = (1.8 \cdot log(Re) - 1.5)^2 \tag{2}$$

The power P_{pump} which is required to drive the coolant mass flow $\dot{m}_{coolant}$ against the channel pressure drop $\Delta p_{channel}$, is calculated by Equation 3, with the help of the loss coefficient ξ (Equation 4). For the channel U-bends, a loss factor ξ of 1.7 is used (Gnielinski, 2013).

$$P_{cooling} = \dot{V}_{coolant} \cdot \Delta p = \frac{\dot{m}_{coolant}}{\rho} \cdot \Delta p \qquad \text{with} \qquad \Delta p = \xi \frac{\rho u^2}{2} \tag{3}$$

$$\xi_{lam} = \frac{64}{Re} \quad \text{for} \quad Re < 2,300 \qquad \text{or} \qquad \xi_{turb} = \frac{0.3146}{\sqrt[4]{Re}} \quad \text{for} \quad Re >= 2,300 \tag{4}$$

To account for the increase in coolant temperature in the stream-wise direction, the cooling channel is divided into multiple sections. For each channel section i, the area-averaged blade-surface temperature is specified as the channel wall temperature T_{wall} and the heat flux $\dot{q}_i$ over the section surface area A_i is calculated by Equation 5 with the incoming coolant temperature $T_{fluid,i-1}$. The heat transfer coefficient α is predicted by Equation 1 or 2.

$$\dot{Q}_i = A \cdot \dot{q} \quad \text{with} \quad \dot{q}_i = \alpha \cdot (T_{fluid,i-1} - T_{wall,i}) \quad \text{and} \quad T_{fluid,i} = T_{fluid,i-1} + \frac{\dot{Q}_{i-1}}{\dot{m} \cdot c_p} \tag{5}$$

Model Plausibility Check

The comparison in Figure 4 shows a good agreement between the one-dimensional prediction and the three-dimensional CFD results. As can be expected from Equation 3, the pressure loss increases by the square of the coolant mass flow, while the heat flux increases linearly (Figure 4). The deviation between both models is deemed to be accurate enough for further parametric studies.

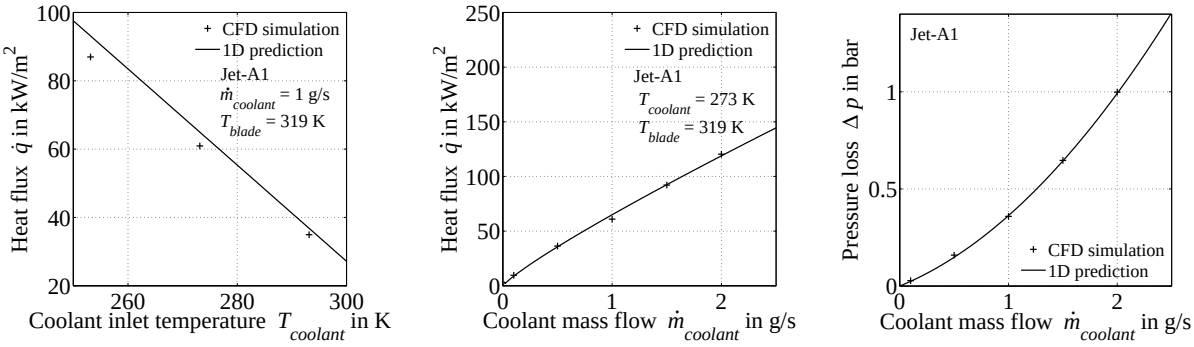

(a) Heat flux (coolant temperature) (b) Heat flux (coolant mass flow) (c) Pressure loss

Figure 4: **Comparison of one-dimensional predictions to three-dimensional CFD results**

Evaluation of Possible Cooling Combinations

Internal to the blade, the coolant flow can be directed concurrently from the leading to the trailing edge or counter-currently with respect to the compressor main flow direction. Counter-current coolant flow gives the highest heat transfer rate. Because of its superior cooling-to-pumping-power ratio with respect to air and kerosene, water is considered as coolant for the following investigations.

For a coolant supply for individual blades of the same stator row, the two available options are to supply each blade in *parallel* with coolant with the same low inlet temperature, or to supply a *series* of succeeding blades with coolant flow which has been preheated from preceding blades. The coolant flow through multiple stator rows of a multi-stage axial compressor can be directed concurrently from the compressor inlet to the outlet or in the opposite direction. The heat which is absorbed by means of water-cooled stator blades in different cooling combinations is listed in Table 4. The results show that a counter-current coolant flow through the compressor with serial stator connection only cools the rear stages, and heats the front stages. A maximum total cooling rate of 11 kW is achievable if each blade is supplied separately with coolant. Thermal connection of stages in a series reduces the heat extraction by 50%, but gives a nearly constant cooling rate of approx. 1.9 kW in each stage.

Figure 5 shows the coolant inflow temperature to successive blades for the serial cooling configurations from Table 4. In each case, a maximum of four blades in each stator can be cooled before the coolant temperature reaches the blade surface temperature. As mentioned above, in a counter-current cooling configuration, the coolant will be cooled by the compressor main flow in the front stages (Figure 5(c)).

ANALYSIS OF A SINLGE STAGE WITH AN INTERNALLY-COOLED STATOR

To evaluate the influence of cooling on the stage performance in terms of stage pressure ratio and isentropic stage efficiency, the second stage is equipped with an internally water-cooled

Table 4: **Heat absorbed by water in Watt for various cooling configurations (1 g/s of water with 283K inlet temperature)**

No.	Global coolant flow direction	Inter-blade connection	Inter-stage connection	Stage 1	Stage 2	Stage 3	Total
1	concurrent	parallel	parallel	2,012	3,775	5,513	11,301
2	concurrent	serial	parallel	86	153	224	464
3	concurrent	parallel	serial	2,012	1,720	1,816	5,549
4	concurrent	serial	serial	86	68	70	224
5	counter-current	parallel	serial	-1,649	-1,050	5,513	2,814
6	counter-current	serial	serial	-68	-69	224	86

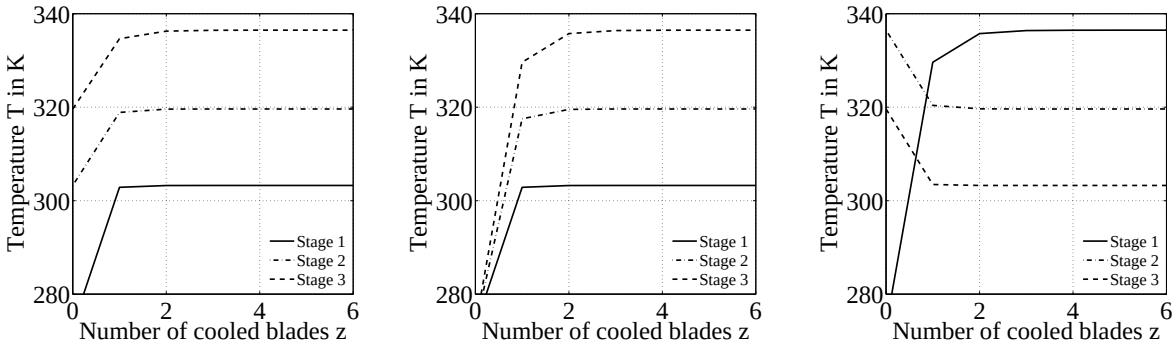

(a) Configuration 2 (b) Configuration 4 (c) Configuration 5

Figure 5: **Coolant inflow temperature for various cooling configurations from Table 4**

stator blade row. The stator row is the same which was used in the previous analyses.

Numerical Setup

For three-dimensional CFD simulation of the cooled compressor stage, *Numeca FINE/Turbo* is used with a one-million node mesh per blade passage generated with *Numeca AutoGrid5*, modeling a fully turbulent flow with the *Spalart-Allamaras* turbulence model. Conjugate heat transfer is enforced by a constant area-averaged blade-surface heat flux from the single-blade simulations for a coolant mass flow of 1 g/s of water at 10°C. The coolant temperature is chosen to be 10 K above 0°C to avoid freezing. Directly mapped two-dimensional heat-flux distributions from the single-blade simulations lead to solver instabilities. A thermal equilibrium state between the single-blade model and the single-stage model is achieved by a balance between the averaged blade-surface temperature and the heat flux ("thermal blade-to-stage coupling"). For this purpose, the wall-temperature dependent heat flux of the blade solid is balanced by the heat-flux dependent wall temperature of the compressor stage. For this purpose, the cooled blade and the cooled stage are simulated separately for different operating points in order to obtain the temperature-heat flux correlation for each configurations. The intersections of the blade and stage correlations indicate the states of thermal balance. Numerical validation of these intersection points yields a relative accuracy of 0.2 % in terms of compressor mass flow.

Results

With respect to the adiabatic compressor, Figure 6(b) demonstrates that neglecting the thermal blade-to-stage coupling leads to a predicted increase in stage efficiency by 2.44% whereas

consideration of thermal coupling reduces the stage-efficiency gain by cooling to 1.26%. The positive effect of cooling on the stage efficiency extends over the complete operating range. The stage pressure ratio is not influenced by cooling (Figure 6(a)). Despite this high impact on stage performance, Figure 6(c) reveals that the aerothermal effect of internal blade cooling is spatially very limited to the blade wake and boundary layers. Blade cooling reduces the flow temperature and accelerates the blade boundary-layer flow only in this narrow region.

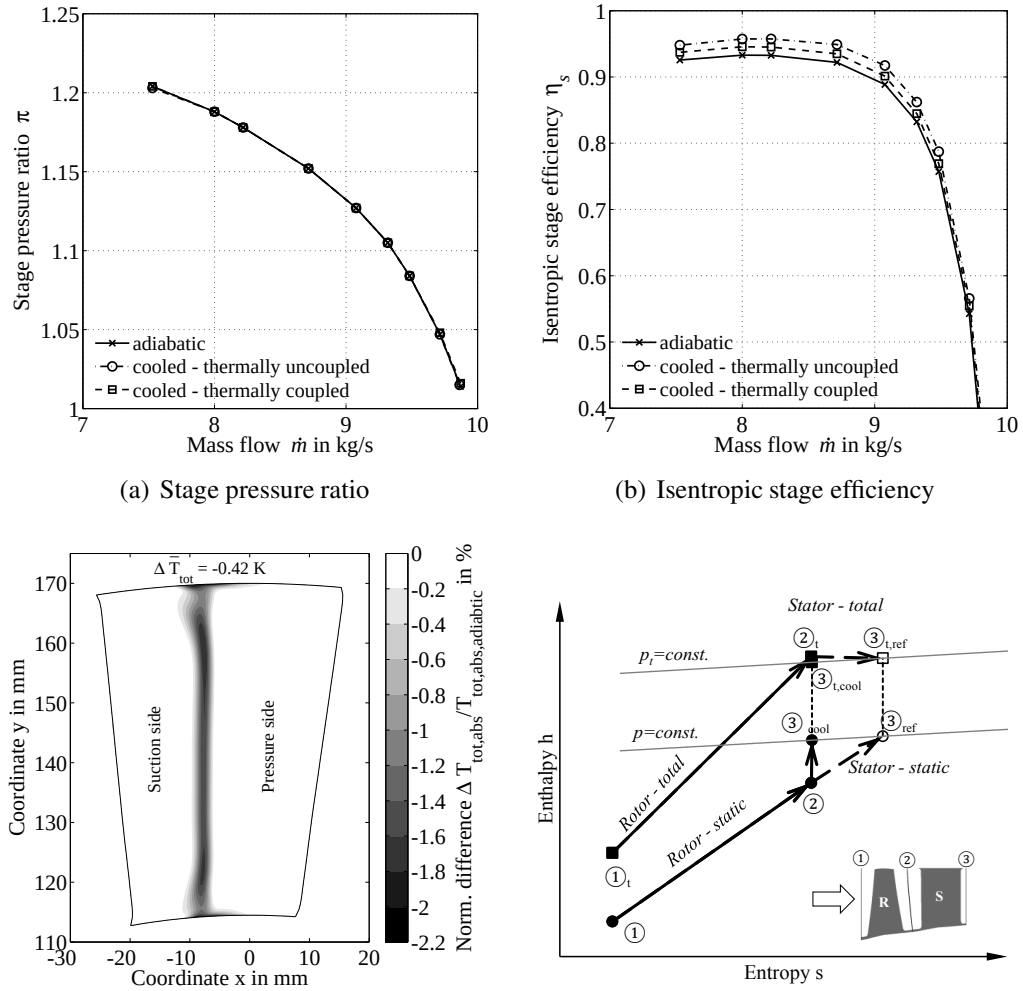

(a) Stage pressure ratio

(b) Isentropic stage efficiency

(c) Stator outlet-flow temperature

(d) Enthalpy-entropy diagram

Figure 6: **Cooling effects on stage performance and stator outlet-flow conditions**

Figure 6 shows that stator cooling does not change the stage pressure ratio significantly, but that it increases the stage efficiency. Because the stator flow is subsonic, the cooling inside the blade passage principally can influence the flow conditions upstream and downstream of the stator row, which most probably would change the incidence or deviation angle. Both effects are not apparent, because the pressure ratio remains unchanged. Nevertheless, the isentropic efficiency of a cooled compressor stage does not only depend on the total pressure loss, but on the heat exchange as well. Since the stage inlet conditions e.g. total temperature and total pressure are independent of stator cooling, and the pressure ratio indicates insignificant changes of the pressure loss, the stage efficiency depends only on the outlet total temperature. Thus, the increase in stage efficiency mainly results from the thermal effect of a reduced outlet total

Table 5: **Cooling effect on stage and compressor efficiency**

$\Delta\eta$	Stage 1	Stage 2	Stage 3	Compressor
Cooling of stage 2	+0.00%	+1.71%	-0.41%	+0.45%
Cooling of all stages	+2.09%	+1.15%	+0.91%	+1.45%

Table 6: **Cooling effect on stage and compressor pressure ratio**

$\Delta\pi/\pi_{ref}$	Stage 1	Stage 2	Stage 3	Compressor
Cooling of stage 2	+0.00%	+0.00%	+0.09%	+0.09%
Cooling of all stages	+0.00%	+0.08%	+0.17%	+0.26%

temperature rather than from a change of the aerodynamic pressure loss.

The enthalpy-entropy diagram (Figure 6(d)) illustrates that the heat extraction by stator cooling results in an isentropic flow deceleration in the stator and consequently in an increased stage efficiency. Moreover. it reveals the high degree of reaction of the aerodynamic stage design and suggests that a lower degree of reaction or a higher stator loading respectively might be crucial for increasing the beneficial stator-cooling effect on the stage efficiency.

ANALYSIS OF A THREE-STAGE AXIAL COMPRESSOR WITH COOLED STATORS

Numerical Setup

The numerical setup of the complete three-stage compressor is analogous to the water-cooled single-stage setup. Area-averaged heat fluxes for each stage are predicted by the one-dimensional model for cooling configuration 1 (Table 4) and mapped on the blade surface.

Results

Table 5 shows that the efficiency gain of +1.71% from the second-stage cooling is reduced to an compressor efficiency increase of 0.45% because of stage mismatching and an efficiency penalty of -0.41% in the third stage. Cooling of all stages results in a compressor-efficiency elevation of +1.45%. Although all stages profit from internal blade cooling in terms of efficiency, the positive cooling effect is mitigated partially by stage-mismatching. In an embedded cooled stage, the second stage efficiency is increases by +1.15% instead of +1.71% not only because of altered inflow conditions from the first cooled stage, but also because of a lower temperature of the pre-cooled air flow. One result of cooling the upstream stages is that the rear stages change their aerodynamic operating point. For a lower inlet temperature, the aerodynamic operating point of the rear stages shifts towards a higher corrected rotational speed $N/\sqrt{T}$ as well as to a lower corrected mass flow $\dot{m}\sqrt{T}/p$, and thus towards a lower efficiency (Tables 5 to 8).

One approach to increase the thermal efficiency gain from internal stator-blade cooling is to increase the heat-exchanging surface (Equation 5). This results in a larger chord length and/or more blades, which means a higher stator solidity. The aerodynamic drawback of this approach might be increased blade losses because of an increase in wetted blade surface. To fundamentally elaborate which of these two effects is dominant, the solidity-dependent losses at mid-span are empirically predicted with loss correlations for circular *NACA-65* cascades (Robbins et al., 1965), which are modified by the cooling influence predicted by numerical flow

Table 7: **Cooling effect on corrected rotational speed**

$\Delta N_{aero}/N_{aeo,ref}$ $N_{aero} \sim N/\sqrt{T_1}$	Stage 1	Stage 2	Stage 3	Compressor
Cooling of stage 2	+0.00%	+0.00%	+0.05%	+0.00%
Cooling of all stages	+0.00%	+0.05%	+0.10%	+0.00%

Table 8: **Cooling effect on corrected mass flow**

$\Delta\dot{m}_{aero}/\dot{m}_{aero,ref}$ $\dot{m}_{aero} \sim \dot{m}\sqrt{T_1}/p_1$	Stage 1	Stage 2	Stage 3	Compressor
Cooling of stage 2	+0.00%	+0.00%	-0.05%	+0.00%
Cooling of all stages	+0.00%	-0.05%	-0.23%	+0.00%

simulations. Under the assumption that the blade design is adapted to the flow conditions from cooled compressor stages, Figure 7 reveals that the stage efficiency increases with higher stator solidity. This means that for the investigated baseline compressor (Table 1), the efficiency under the influence of stator cooling is dominated by the thermal benefits from cooling and not by the aerodynamic deficits from increased blade losses.

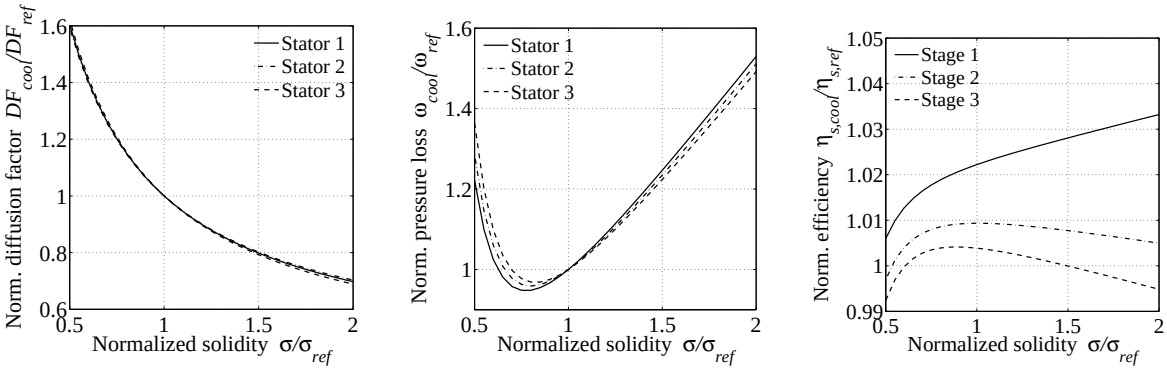

(a) Diffusion factor (b) Loss coefficient (c) Stage efficiency

Figure 7: **Effect of stator solidity on stage performance under cooling influence**

EFFECT OF INTERNAL STATOR COOLING ON THE GAS-TURBINE EFFICIENCY

So far, the positive effects of blade cooling on efficiency were considered only in the limited framework of a stage or a compressor. The final question is: how large is the influence on the gas-turbine thermal efficiency, taking into consideration the power for supplying the coolant. For this reason, the thermal efficiency for a representative gas turbine is modified by the effects of cooling. Figure 8 shows a prediction of the change in thermal efficiency as a function of isentropic total-to-total compressor efficiency with and without recuperation of the heat extracted from the compressor flow. The power for coolant supply is calculated from Equation 3 for water cooling, and accounted for in the efficiency calculation. Without recuperation, Figure 8 predicts a linear increase in normalized cycle efficiency, which is approximately identical to the increase in normalized compressor efficiency. With recuperation, the gain in cycle efficiency is twice

the gain in compressor efficiency. One approach to recuperate the heat which is extracted from the compressor is the preheating of kerosene before it enters the combustion chamber. In some engine configurations, the cold kerosene (approx. -37°C) from the tank must be preheated by cooling of hydraulic system components to keep it liquid. At high flight altitudes e.g. 11 km, the ambient temperature of -57°C is well below the freezing temperature of kerosene (-40°C). Thus, recuperation by kerosene preheating would reduce the heat amount which must be spent solely on heating up the fuel droplets before ignition.

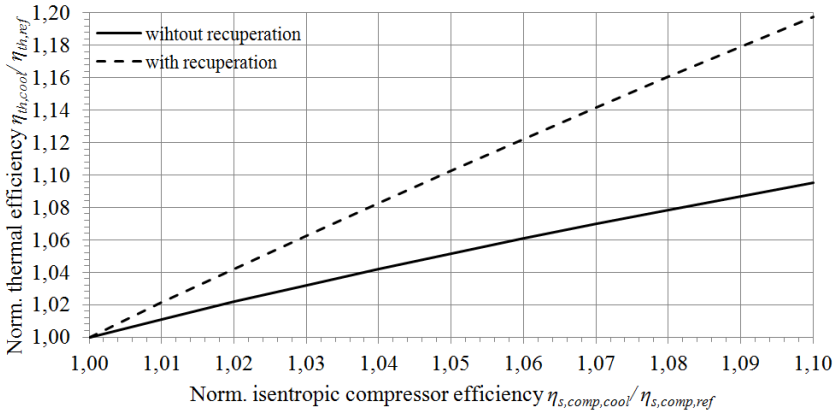

Figure 8: **Effect of compressor efficiency on gas turbine thermal efficiency**

CONCLUSIONS

For a given pumping power, which is required to supply an internal coolant flow, water has the highest cooling-to-pumping-power ratio of 700, while kerosene and air reach only 35% and 5% of this cooling capability respectively. For internally water-cooled stator blades under realistic boundary conditions, the results from numerical simulations predict an isentropic total-to-total stage efficiency increase by 1.26 percentage points and no effect on the stage pressure ratio. For a multi-stage axial compressor with internal stator-blade cooling, the overall efficiency could be increased by 1.45 percentage points. Since stator blade cooling changes the flow conditions for downstream blade rows, the rear stages change their aerodynamic operating point. Without a suitable adoption of the stage matching to compressor cooling, the latter effect puts an aerodynamic penalty on the thermal gain in compressor efficiency by stator cooling.

The chosen profile-thickness distribution and the maximum thickness are aerodynamic design parameters, which set obvious limits to the spatial extend of the cooled blade surface. With a focus on low thermal resistance and a maximum cooling-influenced surface area, profiles with a minimum and constant thickness distribution seem most promising for maximum heat exchange at lowest pressure loss. With respect to the cooling system design, a concurrent cooling system with blade-stage-individual coolant supply gives maximum cooling rates in each stage and in total. A concurrent cooling system with blade-individual and stage-serial coolant supply results in reduced but stage-uniform cooling rates.

Aero-thermal engineering options to increase the benefits of stator-blade cooling are:

1. Maximize the blade surface heat transfer but consider increased blade loss.
2. Increase the coolant mass flow but consider increased pressure loss.
3. Maximize the driving temperature gradient but consider additional thermal blade stress.

A higher blade surface heat transfer directly results in higher stator solidity, in case of a pitch reduction by more blades or longer blade chords. Preliminary empirical predictions indicate that for a higher stator solidy, the stage-efficiency increase from cooling can only be maximized further if the change in flow angle is considered by means of blade-angle adoption. Besides a larger blade surface area, a higher stator solidity allows stronger flow diffusion which leads to higher wall temperature gradients within the adiabatic stator flow passage.

Further, external cooling techniques should be considered. A combination of active flow control by injection and film cooling might hold additional potentials for thermal improvements in combination with aerodynamic flow stabilization.

An important engineering issue which has not been addressed yet, is the impact of additional thermal stress on structural integrity in internally cooled compressor stator blades. It is obvious that cooled stator blades are more highly loaded than adiabatic blades, but from the authors' general judgment, stator blades seem to have higher unused strength reserves than rotor blades of identical blade dimensions.

Though in general stator cooling seems to be applicable in industrial gas turbines as well as in aero engines, the latter application demands for a weight-reduced cooling system. To give a first impression of the expected weight of a water-based cooling system, the additional weight of cooling water and equipment (tank, pump, pipes, heat exchanger) is estimated with similar components from the lubrication system of a decommissioned jet engine. The additional engine weight for single-stage cooling is estimated to be 106% of the lubrication-system weight. Main contributor to this weight increase is a 40l-reservoir for the coolant. In case of the reference jet engine, the basic system which is required for cooling a single compressor stage would increase the engine weight by 0.3%. Assuming a power-independent pump weight, each additional cooled stage would come at the costs of additional water-filled pipes and the blade-internal water content. These sum up to a 0.12% increase in engine-weight per cooled stage. Nevertheless, internal compressor blade cooling should be further evaluated in terms of additional engine weight versus increased cycle efficiency, and lower specific fuel consumption to find an optimum between these competing design objectives of aircraft engines.

REFERENCES

Gnielinski, V. (2013). On heat transfer in tubes. *Int. J. Heat Mass Transfer*, 63:134–140.

Han, J.-C., Dutta, S., and Ekkad, S. (2013). *Gas turbine heat transfer and cooling technology*. CRC Press.

Robbins, W., Jackson, R., and Lieblein, S. (1965). Blade-element flow in annular cascades. In Johnson, I. A. and Bullock, R. O., editors, *Aerodynamic Design of Axial-Flow Compressors (NASA SP-36)*, pages 227–254. NASA, Washington.

Shah, P. N. and Tan, C. (2007). Effect of blade passage surface heat extraction on axial compressor performance. *J. Turbomachinery*, 129(3):457–467.

Sieber, J. (2015). *NEWAC Technologies - Highly Innovative Technologies for Future Aero Engines*. MTU Aero Engines GmbH.